ROYAL SOCIETY
OF CHEMISTRY

PAPER

Check for updates

Peripheral halogen atoms in multi-resonant thermally activated delayed fluorescence emitters: the role of heavy atoms in intermolecular interactions and spin orbit coupling†‡

Hector Miranda-Salinas, [ID] §[a] Jingxiang Wang,§[b] Andrew Danos, [ID] [a] Tomas Matulaitis,[b] Kleitos Stavrou, [ID] *[a] Andrew P. Monkman [ID] *[a] and Eli Zysman-Colman [ID] *[b]

Multi-resonant thermally activated delayed fluorescence materials (MR-TADF) can show narrow-band emission with high photoluminescence quantum efficiency, desirable for applications in organic light emitting diodes (OLEDS). However, they frequently suffer from slow reverse intersystem crossing (RISC) compared to established donor–acceptor TADF emitters, leading to severe device efficiency roll-off at high exciton densities. Introducing heavy atom effects (HAE) by core-substitution has been previously shown to enhance spin orbit coupling and thus RISC in MR-TADF emitters, frequently with oxygen atoms replaced by isoelectronic sulfur or selenium. Here, we explore an alternate HAE strategy using peripheral halogenation of the MR-TADF **DiKTa** core, comparing *t*Br-**DiKTa** and **dBr-*t*Bu-DiKTa** with non-halogenated **Mes₃-DiKTa**. The two brominated emitters demonstrate improved k_{RISC} because of the HAE, while the rate appears to improve by an additional order of magnitude in the mCP host, because of intermolecular (guest–host) interactions. Despite the beneficial hetero-intermolecular interactions, strong homo-intermolecular interactions result in enhanced non-radiative pathways and lower photoluminescence quantum yields. OLEDs of **dBr-*t*Bu-DiKTa** hence showed comparable EQE_{max} with **Mes₃-DiKTa** (21%) and improved efficiency roll-off until 500 cd m^{-2}, although with accelerated roll-off beyond a critical current density. Together with comparisons in less heavily doped devices, these results show that the HAE provided by peripheral halogens improves the device performance up to 500 cd m^{-2}, but also supports detrimental intermolecular interactions that dominate at higher device currents.

[a] *Department of Physics, Durham University, Durham, UK DH1 3LE.*
E-mail: a.p.monkman@durham.ac.uk, kleitos.stavrou@durham.ac.uk

[b] *Organic Semiconductor Centre, EaStCHEMSchool of Chemistry, University of St Andrews, St Andrews, UK KY16 9ST. E-mail: eli.zysman-colman@st-andrews.ac.uk*

† Electronic supplementary information (ESI) available: NMR, HRMS and HPLC of **dBr-*t*Bu-DiKTa**. Cyclic voltammetry. Supplementary computational data for **dBr-*t*Bu-DiKTa**, *t*Br-**DiKTa** and **Mes₃-DiKTa**. Extended HAE TADF emitter literature study. Additional photophysical and OLED data. See DOI: https://doi.org/10.1039/d3tc04394k

‡ The research data supporting this publication can be accessed at https://doi.org/10.17630/9bf6dac8-33d7-409e-b0c6-8ee2e5be708e.

§ These authors contributed equally.

Introduction

Organic light-emitting diodes (OLEDs) have emerged as an important alternative to traditional light-emitting devices such as LCDs.[1,2] Amongst their advantages, OLEDs are self-emissive and addressable on the scale of single pixels, and so do not require a backlighting panel. As a result, they are energy efficient, and can produce pure black with high contrast.

Furthermore, they are also able to be fabricated on a multitude of diverse substrates opening the door to very thin, foldable/rollable and even semi-transparent displays.[3]

The first-generation of OLEDs used fluorescent emitters and thus were limited to a maximum internal quantum efficiency (IQE) of 25%, as only the singlet excitons could produce light. The two main classes of compounds used to raise this efficiency ceiling to 100% IQE are organometallic phosphorescent (Ph) complexes (used in most current commercialized OLEDs) and more recent thermally activated delayed fluorescence (TADF) emitters. In PhOLEDs singlet excitons are converted to triplet excitons, all of which phosphoresce with the assistance of the heavy metal ion, which promotes strong spin–orbit coupling (SOC) facilitating both intersystem crossing (ISC) and phosphorescence emission.[4,5] In TADF OLEDs, triplet excitons are up-converted to singlet excitons by reverse intersystem crossing (RISC), all of which may then fluoresce.[6,7] TADF is possible when there is both a sufficiently small singlet–triplet energy gap (ΔE_{ST}) and non-zero SOC between the relevant singlet and triplet states of different orbital types.

1996 | *J. Mater. Chem. C,* 2024, **12**, 1996–2006

This journal is © The Royal Society of Chemistry 2024

One of the key metrics of TADF materials that affects device performance is the rate of RISC. Rapid RISC (large k_{RISC}) implies the efficient harvesting of triplet excitons and their conversion to singlets, outcompeting both intrinsic non-radiative pathways (increasing an OLED's IQE and stability) as well as multi-excitonic quenching pathways such as triplet–triplet annihilation, and thereby alleviating the efficiency roll-off of the external quantum efficiency (EQE) at higher driving current (where triplet exciton density is the highest). According to Fermi's Golden rule, the rate of RISC can be expressed according to eqn (1):[8]

$$k_{RISC} \propto |H_{SO}|^2 \exp\left(-\frac{\Delta E_{ST}}{k_B T}\right) \quad (1)$$

where k_B, H_{SO}, ΔE_{ST} and T refer to Boltzmann's constant, spin–orbit coupling (SOC) matrix element, the singlet–triplet energy gap, and temperature, respectively. Thus, a small energy difference between the coupled triplet and singlet states (small ΔE_{ST}) and strong SOC are synergistically effective to obtain a fast k_{RISC}.

Many strategies have been developed to increase the k_{RISC}.[9] For example, extending the π-skeleton and charge delocalization in MR-TADF emitters can reduce the ΔE_{ST} of MR-TADF emitters.[10–12] Introducing a long-range charge transfer character into the emissive excited state by decorating the MR-TADF core with peripheral donors has also been shown to reduce the ΔE_{ST} and enhance SOC.[13–16] As SOC is approximately proportional to the fourth power of the nuclear charge of the atoms involved in the emissive transition, another strategy that has been effectively used to enhance k_{RISC} in TADF molecules is to introduce heavy atoms to enhance the SOC.[17] Halogenation of donor–acceptor (D–A) TADF molecules (e.g. with Cl, Br, and I) is a common strategy to enhance SOC. Bunz et al. first reported the exploitation of the internal heavy atom effect (HAE) in TADF compounds by decorating halogen atoms onto carbazole donors in multi-carbazole TADF emitters. With increasing numbers of bromine and iodine substituents, the excited-state lifetimes were found to be considerably shortened. Octaiodo derivatives **3f** and **5f** exhibited the shortest lifetimes of 1.2 and 0.4 μs respectively (Fig. 1). Although the photoluminescence quantum yields (Φ_{PL}) were slightly decreased, halogen substituents were effective at accelerating both ISC and RISC.[18] Kim et al. carried out both theoretical and experimental studies of halogenated analogues of **4CzIPN**. **4CzIPN-Cl**, **4CzIPN-Br**, and **4CzIPN-I** showed increased calculated SOC matrix elements (SOCME) between S_1 and T_1, of 0.24, 0.51, and 1.09 cm^{-1}, respectively compared to **4CzIPN** (0.22 cm^{-1}). Consequently, both k_{ISC} and k_{RISC} increased, with **4CzIPN-I** having the fastest k_{ISC} and k_{RISC} of 1.10×10^9 and 9.05×10^7 s^{-1}, respectively. However, the OLEDs based on these materials showed lower maximum EQE (EQE$_{max}$) and more severe efficiency roll-off with the emitters bearing Br and I substituents, demonstrating that the incorporation of heavy elements does not always uniformly translate into an improved device performance. It is reasonable to speculate that weak C–X halogen bonds could lead to electrical instability in the devices. Additionally, faster k_{ISC} (increased in tandem with k_{RISC}) can also compete with radiative singlet decay (k_r^s), resulting in

multiple spin–flip cycles between S_1 and T_1 rather than direct emission following RISC.[19,20] Further examples of HAE investigations of D–A TADF materials are summarised in the (ESI†).[21–31]

In contrast to D–A TADF materials, multi-resonant TADF emitters (MR-TADF) are rigid polycyclic aromatic compounds containing a combination of p- and n-dopants, which usually show larger ΔE_{ST} (>0.10 eV) and slower k_{RISC} ($\sim 10^4$ s^{-1}).[32] RISC is typically enabled through an upper-state crossing mechanism rather than the vibronic coupling of the lower energy triplet states in D–A TADF emitters.[33,34] Introducing heavy atoms into MR-TADF emitters is therefore a promising strategy to address their slower k_{RISC}. Indeed, Chen et al. reported the boron/sulfur-based MR-TADF emitter **BSS** (Fig. 1),[35] which possesses a large SOCME of 0.77 cm^{-1} between the S_1 and T_1 states and a faster k_{RISC} of 1.18×10^5 s^{-1} compared to oxygen-containing analogues **BOS** (SOCME = 0.62 cm^{-1} and $k_{RISC} = 6.1 \times 10^4$ s^{-1}) and **BOO** (SOCME = 0.01 cm^{-1} and $k_{RISC} = 1.1 \times 10^4$ s^{-1}). Additional examples of HAE investigations for MR-TADF emitters are included in the ESI,† although we note that in all cases these involve heavy atom substitution directly within the MR-TADF core.[35–47]

We previously reported the MR-TADF emitter **DiKTa** and its mesitylated congener, **Mes$_3$-DiKTa** (Fig. 1), which showed reduced aggregation-caused quenching and aggregate formation due to the presence of the bulky mesityl groups.[48] Similar to most MR-TADF emitters, **Mes$_3$-DiKTa** showed only moderate k_{RISC} and large ΔE_{ST} in 3.5 wt% doped mCP films. Here, we demonstrate how replacing the three mesityl groups with bromines (**tBr-DiKTa**) leads to both faster k_{RISC} and smaller ΔE_{ST} but stronger intramolecular interactions in the zeonex host. To minimize intermolecular interactions and suppress concentration quenching while still taking advantage of the peripheral halogen HAE, a dibrominated derivative (**dBr-tBu-DiKTa**) was also investigated. Although the heavy atom effect is clear in inert matrices, in the mCP host a competing exciplex formation channel (guest–host interaction) provides an alternate exciton harvesting channel. The improved k_{RISC} and stronger hetero-intermolecular interactions evident in optical measurements of **dBr-tBu-DiKTa** resulted in an EQE$_{max}$ of 21% in OLEDs, similar to the previously reported device with **Mes$_3$-DiKTa**, but with an improved efficiency roll-off until 500 cd m^{-2}. The presence of homo-intermolecular interactions (likely induced by the halogen atoms) and the weaker C–Br bonds led to more severe device roll-off at these higher current densities, counterbalancing the higher performance they can unlock at a lower driving current. These results therefore demonstrate both the advantageous and detrimental features of peripheral halogen decoration on the performance of MR-TADF OLEDs.
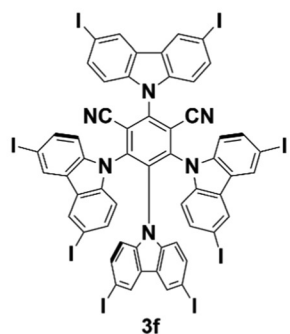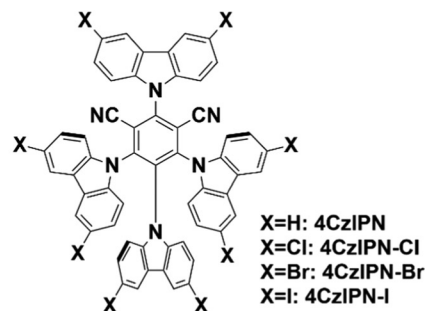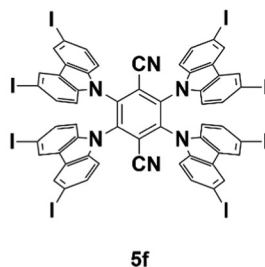
Results & discussion

Synthesis

The synthesis of **dBr-tBu-DiKTa** is outlined in Fig. S1 (ESI†). Intermediate **1** was prepared through high-temperature
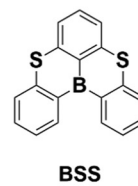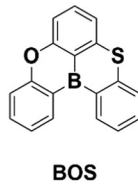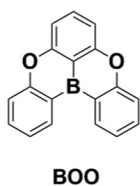
This journal is © The Royal Society of Chemistry 2024

J. Mater. Chem. C, 2024, **12**, 1996–2006 | **1997**
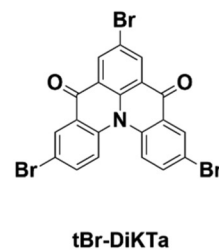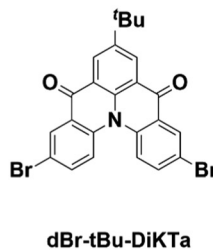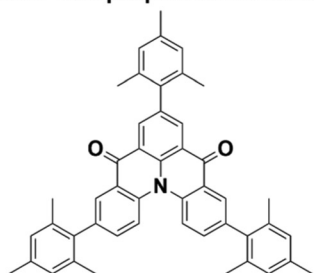
Fig. 1 Structures of selected reported TADF materials with HAE, and the structures investigated in this work (other reported MR-TADF materials with HAE are summarized in the ESI,† p. S24).

Ullmann coupling. This was then brominated in the presence of NBS and hydrolyzed to the diacid intermediate, **3**. Finally, **dBr-*t*Bu-DiKTa** was obtained following a Friedel–Crafts acylation in an overall yield of 32%. **tBr-DiKTa** and **Mes₃-DiKTa** were obtained following the protocols in our previous work.[48] The identity and purity of **dBr-*t*Bu-DiKTa** were confirmed using a combination of NMR, HRMS, EA, HPLC and Mp analyses. Specific synthetic procedures and chemical characterization are provided in the ESI.†

Theoretical calculations

The optimized geometries of the ground and excited states, and the electronic structures of **dBr-*t*Bu-DiKTa**, **tBr-DiKTa**, and **Mes₃-DiKTa** were first calculated using density functional theory (DFT) and time-dependent DFT (TD-DFT) within the Tamm–Dancoff approximation (TDA) at the PBE0/6-31G(d,p) level of theory in the gas phase.[49,50] As shown in Fig. S13 (ESI†),

the LUMO of these materials is located on the **DiKTa** core. The HOMOs are likewise distributed over the **DiKTa** core, and with contributions from the bromine substituents in **dBr-*t*Bu-DiKTa** and **tBr-DiKTa**. There are four low-lying triplet states near or below S_1, which are implicated in facilitating RISC.[33,36,39,51,52] Thus, we calculated the SOC matrix elements (SOCME) for S_1–T_1, S_1–T_2, S_1–T_3, and S_1–T_4 transitions based on the optimized T_1 geometries. With increasing bromine content, SOCME increased from 0.28 to 0.30 and 0.46 cm^{-1} for S_1–T_1, from 5.71 to 13.23 and 22.81 cm^{-1} for S_1–T_2, from 5.59 to 8.45 and 23.23 cm^{-1} for S_1–T_3, and from 8.14 to 26.37 and 33.95 cm^{-1} for S_1–T_4 for **Mes₃-DiKTa**, **dBr-*t*Bu-DiKTa**, and **tBr-DiKTa**, all respectively. The large enhancement of the SOCME values can thus be directly attributed to the HAE.

State energies and difference densities were also calculated using Spin-Component Scaling second-order algebraic diagrammatic construction (SCS-ADC2)/(cc-pVDZ) to provide accurate
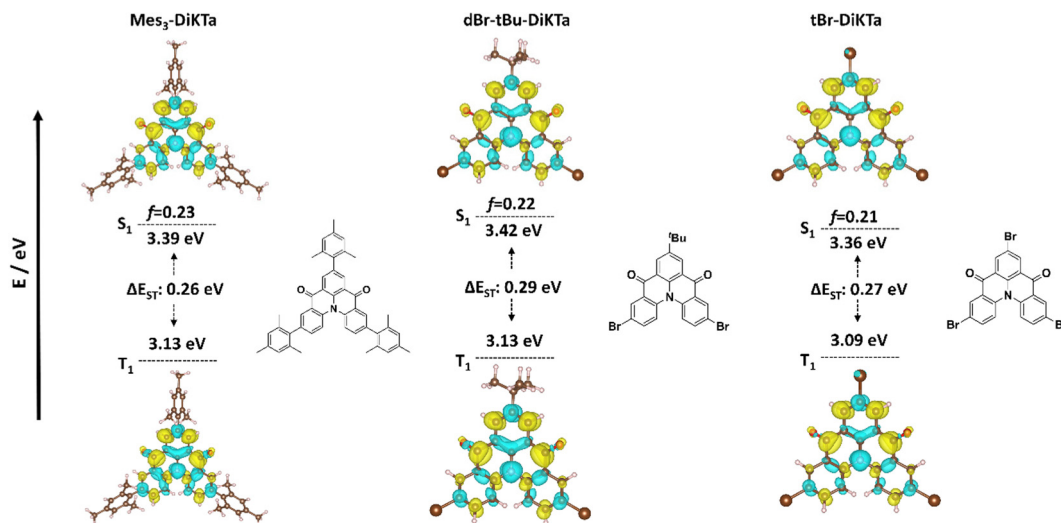
1998 | J. Mater. Chem. C, 2024, 12, 1996–2006

This journal is © The Royal Society of Chemistry 2024

Fig. 2 Difference density plots of S_1 and T_1 for **Mes$_3$-DiKTa**, **dBr-tBu-DiKTa**, and **tBr-DiKTa** calculated in the gas phase using SCS-ADC2 (blue indicates areas of decreasing electron density while yellow indicates increasing electronic density between the ground and excited states).

predictions of the ΔE_{ST} values (Fig. 2).[53,54] All compounds show similar difference density patterns for both S_1 and T_1, localized on the **DiKTa** core and associated with states of short-range charge transfer (SRCT) character. The corresponding ΔE_{ST} values are calculated to be 0.29, 0.27, and 0.26 eV for **dBr-tBu-DiKTa**, **tBr-DiKTa**, and **Mes$_3$-DiKTa**, respectively, which largely reproduce the previously reported values.[48,55]

Electrochemistry

The electrochemical properties of **Mes$_3$-DiKTa**, **dBr-tBu-DiKTa**, and **tBr-DiKTa** were investigated using cyclic voltammetry (CV) and differential pulse voltammetry (DPV) in dichloromethane (DCM). As shown in Fig. S14 (ESI†), due to the inductively electron-withdrawing character of bromine **tBr-DiKTa** and **dBr-tBu-DiKTa** show more anodically shifted oxidation and reduction potentials, and thus more stabilized HOMO and LUMO levels compared to **Mes$_3$-DiKTa**. The oxidation potentials (E_{ox}) and reduction potentials (E_{red}) versus SCE, taken from the peak values of the DPVs, are 1.66, 1.79, 1.81 eV, and −1.39, −1.27, −1.15 eV for **Mes$_3$-DiKTa**, **dBr-tBu-DiKTa**, and **tBr-DiKTa**, respectively. Both **dBr-tBu-DiKTa** and **tBr-DiKTa** also show anodically shifted potentials compared to parent **DiKTa** (E_{ox} at 1.78 V and E_{red} at −1.34 V), again the result of the inductively electron-withdrawing bromine substituents.[55] The corresponding HOMO and LUMO energies are calculated to be −6.00/−2.95, −6.13/−3.07, and −6.15/−3.19 eV, respectively, where the trend matches well with the DFT calculations (Fig. S13, ESI†). The data are summarized in Table S1 (ESI†).

Optical properties

Steady-state absorption and photoluminescence (PL) spectra of **dBr-tBu-DiKTa** and **tBr-DiKTa** in different solvents are shown in Fig. S15 (ESI†). Both absorption and PL spectra undergo a small bathochromic shift (120–150 meV) with increasing solvent polarity, a phenomenon consistent with the short–range charge transfer (SRCT) character of the emissive excited states in

MR-TADF materials.[48,56,57] In toluene (PhMe) solution, the lowest energy absorption maximum of **dBr-tBu-DiKTa** is centred at 445 nm and the main PL peak, λ_{PL}, is at 464 nm. Similar absorption and PL behaviour, at slightly higher wavelengths of 455 and 477 nm, respectively, is observed for **tBr-DiKTa** (Fig. S15b, ESI†).

Comparison of the photophysical properties of **dBr-tBu-DiKTa**, **tBr-DiKTa**, and **Mes$_3$-DiKTa** in the same environment is crucial to understand the effect of the bromine substituents on their ground- and excited-state properties. Fig. 3(a) illustrates this comparison in PhMe solution. The absorption spectral shape is similar in all cases, having a 10 nm peak difference across **dBr-tBu-DiKTa** (445 nm), **Mes$_3$-DiKTa** (449 nm), and **tBr-DiKTa** (455 nm). The molar extinction coefficient, ε, of this lowest energy band is around 5.5×10^4 M^{-1} cm^{-1} in the first two compounds, with **tBr-DiKTa** having a lower value of 3.5×10^4 M^{-1} cm^{-1}. The latter can be explained by the lower oscillator strength of S_1 (0.21 for **tBr-DiKTa** compared to 0.22 for **dBr-tBu-DiKTa** and 0.23 for **Mes$_3$-DiKTa**, Fig. S13, ESI†), as well as the poor solubility of **tBr-DiKTa** leading to ground-state dimer formation even in solution, which reduces the extinction coefficient value. Following the energy trends of the absorption spectra, the PL spectrum of **dBr-tBu-DiKTa** is the bluest with a λ_{PL} of 464 nm, followed by **Mes$_3$-DiKTa** and **tBr-DiKTa** at 472 and 476 nm, respectively. The energetic order of the PL spectra is in reasonably good agreement with the SCS-ADC2 calculations.

Steady-state PL measurements of solution-cast films are shown in Fig. 3(b). At 1 wt% in mCP, **Mes$_3$-DiKTa** and **dBr-tBu-DiKTa** have near-identical PL spectra with λ_{PL} at 483 nm, while **tBr-DiKTa** has a broader PL with λ_{PL} at 488 nm and an additional redshifted feature at 530 nm. A key difference between solution-state and solid-state PL (i.e. in mCP) is that intermolecular (homo- or hetero-molecular) interactions are stronger in the solid state and contribute to the observed emission broadening.[34] Without the steric shielding of the mesityl groups, it is unsurprising that

This journal is © The Royal Society of Chemistry 2024

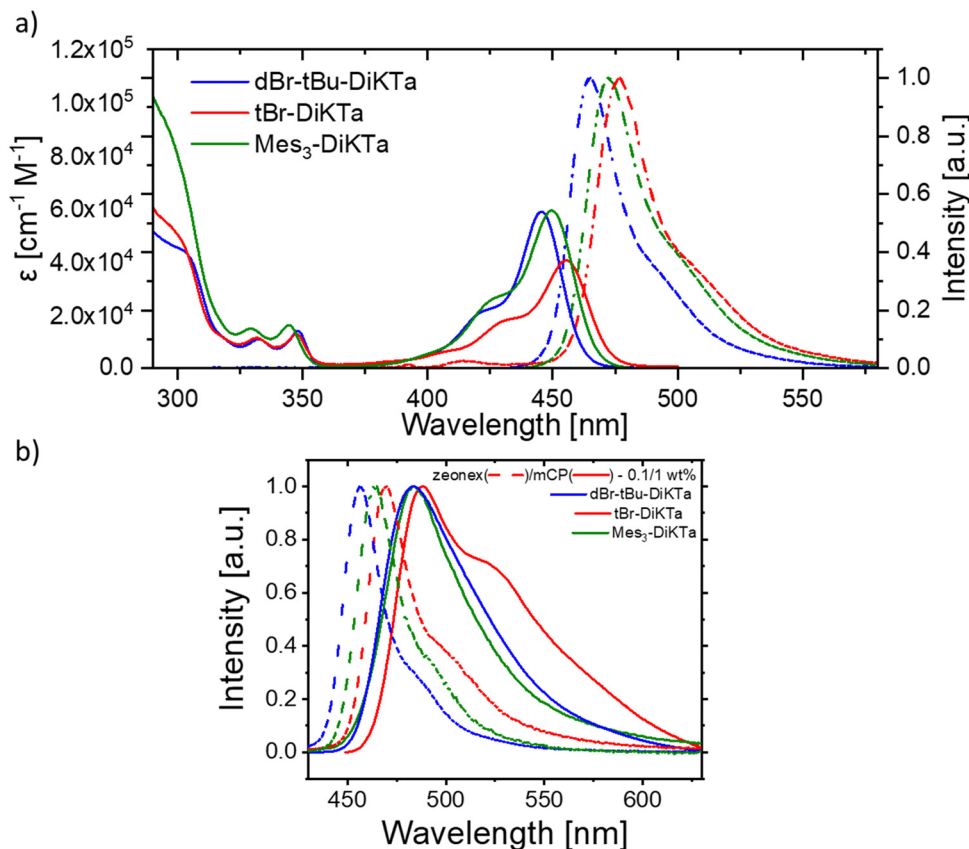J. Mater. Chem. C, 2024, **12**, 1996–2006 | **1999**

Fig. 3 (a) Absorption and normalized steady-state PL of **dBr-*t*Bu-DiKTa**, **tBr-DiKTa** and **Mes₃-DiKTa** in PhMe, at 20 μM concentration (λ_{exc} = 330 nm) and (b) steady-state PL in zeonex (dashed) and mCP (solid) with 0.1 wt% and 1 wt% doping concentrations, respectively.

dBr-*t*Bu-DiKTa interact more compared to **Mes₃-DiKTa**, resulting in a slightly broader and red-shifted emission. **tBr-DiKTa**, which does not contain any sterically bulky groups, appears to interact the most, obvious from the strongest impacts on its PL spectrum.

Doped films at 0.1 wt% of the emitters in zeonex were studied in order to mitigate intermolecular interactions in the solid state (no hetero- and reduced homo-molecular interactions).[34] The PL spectra of these films show similar trends to those observed in solution, with **dBr-*t*Bu-DiKTa** having a λ_{PL} at 456 nm, followed by **Mes₃-DiKTa** at λ_{PL} of 464 nm and **tBr-DiKTa** at λ_{PL} of 470 nm (Fig. 3(b)). With reduced scope for intermolecular interactions in these dilute films, these trends and absence of significant PL broadening help to verify that intermolecular interactions are the main source of spectral broadening in the 1 wt% mCP films. Lower loading in mCP films could not be pursued though, as the thin films with 1 wt% doping were already approaching the lower limits of emission signal sensitivity, in contrast to the much thicker polymeric zeonex films.

Time-resolved PL studies

Time-resolved PL measurements were performed on the same films to investigate the TADF properties of the materials at both 300 K (room temperature) and at 80 K (LT). Previously reported **Mes₃-DiKTa**[48] was used as the benchmark reference material, and diluted in 0.1 wt% zeonex films to allow us to study the

HAEs without significant additional complexity due to intermolecular interactions. The time-resolved decays of the zeonex films are shown in Fig. 4(a). With the introduction of bromine atoms, the prompt fluorescence (PF) and delayed fluorescence (DF) lifetimes become shorter, while the DF contribution to the overall emission increases (Table 1). Thus, **tBr-DiKTa** shows the best TADF response followed by **dBr-*t*Bu-DiKTa** and **Mes₃-DiKTa** – a clear indicator that the peripheral HAE assists in augmenting SOC. Analysis of the decays with fitted exponential lifetimes[58] verifies these trends, with k_{RISC} being higher when more Br atoms are introduced within the emitter (Table 1). Two different methods[6,58] were compared for the decay analysis to explore if the enhanced aggregation (leading to complex decays) affects the calculated rate constants, and the results are broadly similar (Table S2, ESI†).

Although the time-resolved PL decays establish that the presence of the peripheral bromines enhance the TADF performance (through k_{ISC} and k_{RISC}), the greater planarity and electron density of the brominated molecules simultaneously permits an unignorable contribution from aggregates, even at 0.1 wt% concentration in the zeonex matrix. Examining the individual time-resolved PL spectra, those of **Mes₃-DiKTa** show no aggregation contribution at RT, with only a minor contribution at LT manifesting as a broadening of the full width half maximum (FWHM) at the late prompt regime (~50 ns, Fig. S16
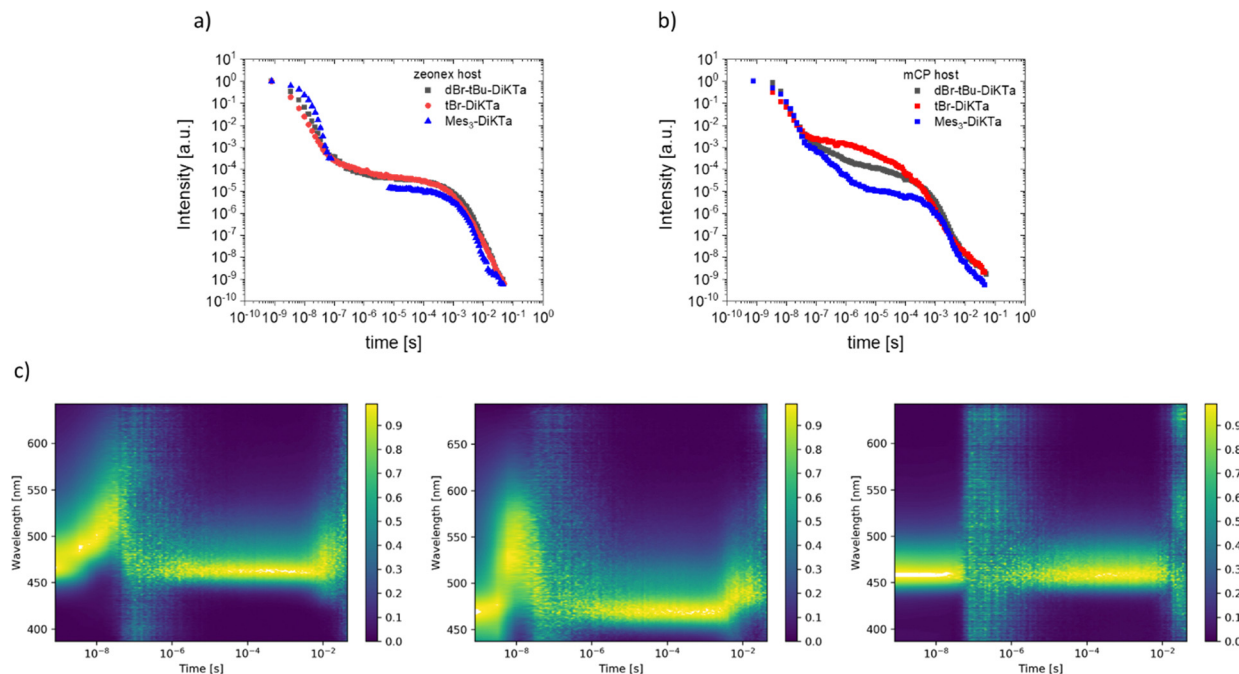
2000 | *J. Mater. Chem. C*, 2024, **12**, 1996–2006

This journal is © The Royal Society of Chemistry 2024

Fig. 4 Time-resolved emission decays of the three molecules in (a) zeonex, at 0.1 wt% and (b) mCP at 1 wt% concentration, at 300 K, and (c) contour plots of **dBr-*t*Bu-DiKTa**, **_t_Br-DiKTa** and **Mes₃-DiKTa** in zeonex films. λ_{exc} = 355 nm.

Table 1 Photophysical data of the three emitters in zeonex (0.1 wt%) and mCP (1 wt%) hosts

Molecule	Host	SS PL[a] [nm]/[eV]	LT PH[b] [eV]	ΔE_{ST}[c] [meV]	τ_{PF}[d] [ns]	[ns]	τ_{DF}[d] [μs]	[μs]	k_{F} [× 10⁸ s⁻¹]	k_{ISC} [× 10⁸ s⁻¹]	k_{RISC} [× 10³ s⁻¹]	Φ_{PL} N₂
_t_Br-DiKTa	zeonex	470/2.64	2.61	140	1.40	6.35	—	755.4	3.86	2.26	4.53	0.23
	mCP	488/2.54	2.52	150	2.99	—	7.01	108.5	3.34	3.53	197	0.61
dBr-*t*Bu-DiKTa	zeonex	456/2.72	2.57	300	2.10	7.23	—	851.3	2.48	1.48	3.63	0.26
	mCP	483/2.57	2.53	210	4.01	—	17.4	310.2	2.49	2.76	19.3	0.82
Mes₃-DiKTa	zeonex	464/2.67	2.55	230	6.79	—	—	912.3	1.47	0.822	1.44	0.53
	mCP	483/2.57	2.51	210	4.55	—	26.68	565.2	2.20	1.35	3.1	0.90

[a] Steady state emission peak. *[b]* Onset energy of the time resolved phosphorescence emission, after 20 ms at 80 K, λ_{exc} = 355 nm. *[c]* ΔE_{ST} estimated from the SS PL and LT PH onset energy. *[d]* From mono- or bi-exponential fitting of PF and DF regions.

and S17, ESI†). The time-resolved PL spectra of **dBr-*t*Bu-DiKTa** instead reveal a stronger aggregation contribution, which appears as a broad, red-shifted emission band from 30–100 ns delay time (Fig. 4(c) and Fig. S18, S19, ESI†). The separate monomer and aggregate emission is well-resolved at lower temperatures, where the monomer-like TADF contribution is suppressed. Similar behaviour with even stronger aggregate emission is observed in **_t_Br-DiKTa**, with the broad time-resolved spectrum dominant in the PF regime (Fig. 4(c) and Fig. S20, S21, ESI†).

To assess the performance of the emitters in a device-compatible host (and at device-relevant concentrations), time-resolved measurements were also performed on 1 wt% mCP films. **Mes₃-DiKTa** at RT in mCP has similar behaviour as in zeonex, indicating that intermolecular interactions remain mostly suppressed. The singlet energy (PL onset) is lower

compared to zeonex films (2.75 and 2.82 eV), likely because of the difference in environment (Fig. S22, ESI†).[59,60] Both PF and DF emission lifetimes are shorter compared to those in zeonex films, consistent with the smaller experimental ΔE_{ST} (230 and 210 meV) and the rigid matrix effect,[61–63] resulting in a two-fold faster k_{RISC} (Table 1). An extra minor decay component in the DF regime is also observed with a lifetime of 26 μs, likely originating from mixed intermolecular and monomer emission (Fig. S22 and S23, ESI†).[64]

Compared to the PL in zeonex, the PL of **dBr-*t*Bu-DiKTa** in mCP changes similarly to that of **Mes₃-DiKTa**, because of the differences in the host environment. An enhanced contribution from a new species appears in the late PF regime (Fig. 5, ~30 ns), observed as a broadened emission that lasts until early μs and is most clearly visible in the contour plot of the normalised time-resolved spectra (Fig. S24, ESI†). Residual host
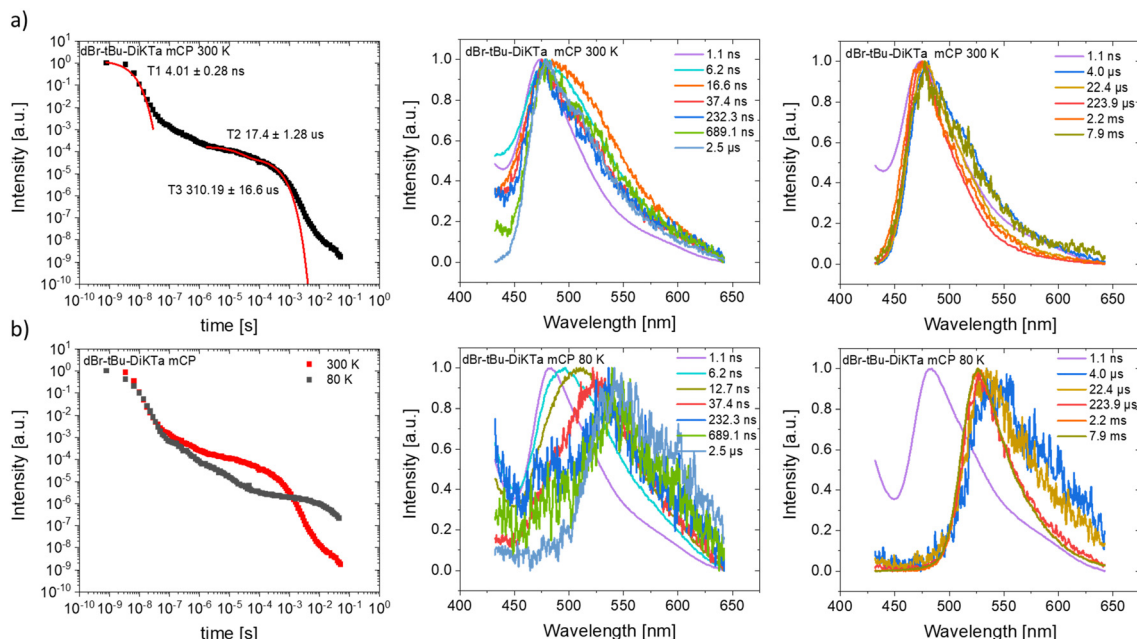
This journal is © The Royal Society of Chemistry 2024

J. Mater. Chem. C, 2024, **12**, 1996–2006 | **2001**

Fig. 5 Time-resolved emission decays and spectra at different time delays, for **dBr-*t*Bu-DiKTa** in a mCP matrix at 1 wt% concentration at (a) 300 K and (b) 80 K. λ_{exc} = 355 nm.

emission from mCP (<400 nm) is also visible in these contour plots during the early PF region, but its contribution is not considered in the time-resolved decay. In the subsequent DF region, the emission becomes narrow again, reflecting a return to pure monomer emission. The intermolecular species contribution dominates at low temperature (where the TADF is completely suppressed) and is coincidentally isoenergetic with the phosphorescence emission. When the room temperature measurement is fitted with exponential lifetimes, the PF has a multi-exponential decay with resolvable components ascribed to both monomer and intermolecular species emission, while the DF lifetime is almost three times shorter compared to zeonex films. As a result, the calculated k_{RISC} becomes over five times faster in mCP (Table 1). The effect of intermolecular interactions is even stronger for ***t*Br-DiKTa** in mCP (Fig. 6 and Fig. S25, ESI†). Like **dBr-*t*Bu-DiKTa**, ***t*Br-DiKTa** PF comprises a mixed monomer and intermolecular species emission, with the latter lasting until early µs. The DF lifetime in mCP becomes seven times shorter than in zeonex, and thus the calculated k_{RISC} appears to be over forty times faster (Table 1).

These big differences in the calculated k_{RISC} for the brominated emitters in the two different hosts at first seem unreasonable, while a second species is clearly involved in the mCP films which complicates the decay kinetics and fitting. The higher emitter concentration in the mCP films also necessarily promotes stronger intermolecular interactions between the guest molecules. In applications, this could either promote a secondary triplet harvesting pathway, or generate a poorly emissive species that quenches the monomer emission.[34,65] To address the latter, different concentrations of **dBr-*t*Bu-DiKTa** (0.1, 1, 4 wt%) in the inert zeonex host (a host with no electronic interaction with the guest molecules)[59] were measured. From the

steady-state measurements, a bathochromic shift of the PL onset is observed along with a broadening of the FWHM with increasing concentration (Fig. S26, ESI†). The red shift is assigned to self-absorption while the increased PL contribution at 480 nm is assigned to aggregate emission. Interestingly, the PL spectrum of the 4 wt% doped film in zeonex is like the one of the 1 wt% doped film in mCP, indicating that the degree of aggregation formation/contribution to the PL spectrum is different in the two hosts. From the time-resolved decays, the monomer prompt lifetime decreases with increasing concentration from 2.1 to 1.5 ns at 0.1 and 4 wt%, respectively, indicating parallel energy transfer from the high-energy monomer to the lower-energy aggregate state. The aggregate prompt lifetime, identified from the different time-resolved PL spectra, increases both in length and contribution (Fig. S19 and S27, ESI†). The delayed emission lifetime also appears to decrease with increasing concentration, from 851 to 274 µs for 1 and 4 wt% doped films of **dBr-*t*Bu-DiKTa**, respectively (Fig. S27a, ESI†). This decrease in prompt and delayed fluorescence lifetimes indicates that the higher emitter concentration leads to stronger intermolecular interactions between the **dBr-*t*Bu-DiKTa** molecules, thus generating poorly emissive aggregate species, considering the low transient signal this species produces. This is also confirmed by the decrease of the Φ_{PL} with increasing **dBr-*t*Bu-DiKTa** concentration (26 and 20% for 0.1 and 1 wt% doped zeonex films, respectively). Thus, the unshielded brominated **DiKTa** molecules have dominant intermolecular interactions at high concentrations, which are at least as impactful as any HAE on the overall photophysics. Nevertheless, at 0.1 wt% with minimal aggregation effects, comparing the three emitters in zeonex hosts reveals the impacts of HAEs on improving the SOC and enhancing the ISC/RISC (Table 1).
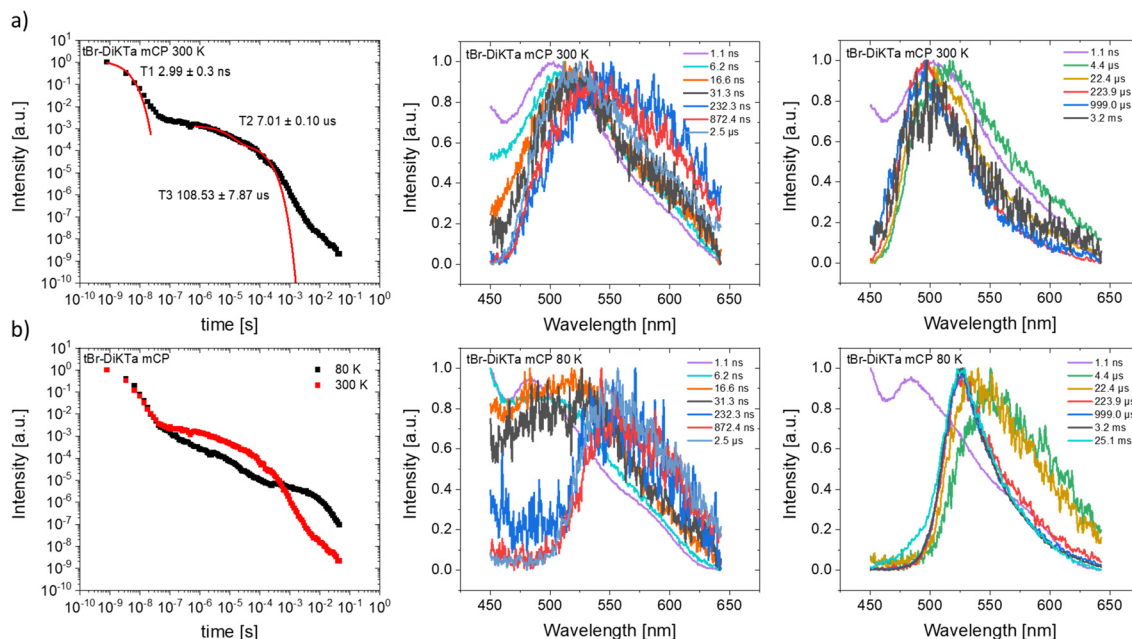
2002 | *J. Mater. Chem. C*, 2024, **12**, 1996–2006

This journal is © The Royal Society of Chemistry 2024

Fig. 6 Time-resolved emission decays and spectra at different time ranges, for **tBr-DiKTa** in a mCP matrix at 1 wt% concentration at (a) 300 K and (b) 80 K. λ_{exc} = 355 nm.

While the Φ_{PL} of 1 wt% zeonex films of **dBr-tBu-DiKTa**, **tBr-DiKTa**, and **Mes₃-DiKTa** are 20, 15, and 47% respectively, these values change dramatically in mCP (1 wt%) to 82, 61, and 90% (Table S2, ESI†). This big difference in Φ_{PL} in the two hosts cannot be explained by guest–guest interactions at such low film doping concentrations. Focusing on **dBr-tBu-DiKTa**, this emitter has a good Φ_{PL} in mCP (promising for devices) but is also sensitive to intermolecular interaction because of its reduced peripheral shielding groups. We observe that the Φ_{PL} for **dBr-tBu-DiKTa** increases to 45% in the UGH-3 host, but this remains far below the 82% measured in mCP. This indicates that the transition to an inert small molecule host (UGH-3) potentially suppresses vibrational motions that may be more active in the more fluid zeonex host (Φ_{PL} 20%). Still, the large mCP Φ_{PLS} cannot be fully explained, and we suggest that it originates from intermolecular interaction between the guest and host molecules, forming an exciplex species.[66] Hetero-molecular interactions are possible based on the measured HOMO/LUMO values of the three emitters (−6.13/−3.07, −6.15/−3.19, and −6.00/−2.95 eV for **dBr-tBu-DiKTa**, **tBr-DiKTa**, and **Mes₃-DiKTa** respectively) and the mCP host (−5.9/−2.4 eV).[67] This energetic difference and non-nested HOMO/LUMOs favour the formation of an exciplex between the two molecules but unfortunately this kind of species has been difficult to observe experimentally because of the parallel presence of aggregates. The presence of an exciplex would also explain the big difference between the PL spectra of the three molecules in mCP (Fig. 3(b)), which have different PL energetic order (**Mes₃-DiKTa** → **dBr-tBu-DiKTa** → **tBr-DiKTa**) compared to solution samples and zeonex films (**dBr-tBu-DiKTa** → **Mes₃-DiKTa** → **tBr-DiKTa**). Furthermore, the absence of the short DF component in zeonex, compared to mCP, is explained by

zeonex not containing any electron-donating fragments (such as carbazole in mCP) that could establish an exciplex state with the DiKTa core.

The complicated co-existence of monomer, aggregate, and exciplex emission in the mCP host makes it difficult to distinguish the spectrum of each individual species. This nuanced situation makes it impossible to calculate the real kinetics of these systems. Thus, the calculated kinetics values do not represent the truth, but an estimation of the systems modelled as single species environments.

Devices

OLEDs using the reference material **Mes₃-DiKTa** have been reported to have an EQE_max of 21.1%, with λ_{EL} = 480 nm and a FWHM of 36 nm.[48] Similar to many MR-TADF devices, these showed a severe efficiency roll-off with an EQE_1000 of 4.5%, likely due to the slow emitter k_{RISC}. Herein, devices using a stack of ITO (anode)|NPB (HTL, 40 nm)|mCP (EBL, 10 nm)|e-mitter:mCP 3.5 wt% (EML, 30 nm)|T2T (HBL, 10 nm)|T2T:LiQ 45% (ETL, 35 nm)|LiQ (1 nm)|Al (cathode, 100 nm) were fabricated using **Mes₃-DiKTa** or **dBr-tBu-DiKTa** as the emitter, with a representative performance shown in Fig. 7; devices with **tBr-DiKTa** were not investigated due to the significantly lower Φ_{PL} of the emitter and its strong aggregation formation.

The devices show good efficiency with EQE_max of 21.2 and 21.6% for the OLEDs with **dBr-tBu-DiKTa** and **Mes₃-DiKTa**, respectively. The device with **dBr-tBu-DiKTa** has a slightly broader EL spectrum (FWHM 54 nm, Fig. 7(c)) compared to the **Mes₃-DiKTa** device, following the PL of the mCP films (Fig. 3(b)), and indicating increased EL contribution from the intermolecular species (Fig. 7(c)). Considering that aggregate formation acts as a quenching contribution to **dBr-tBu-DiKTa**'s
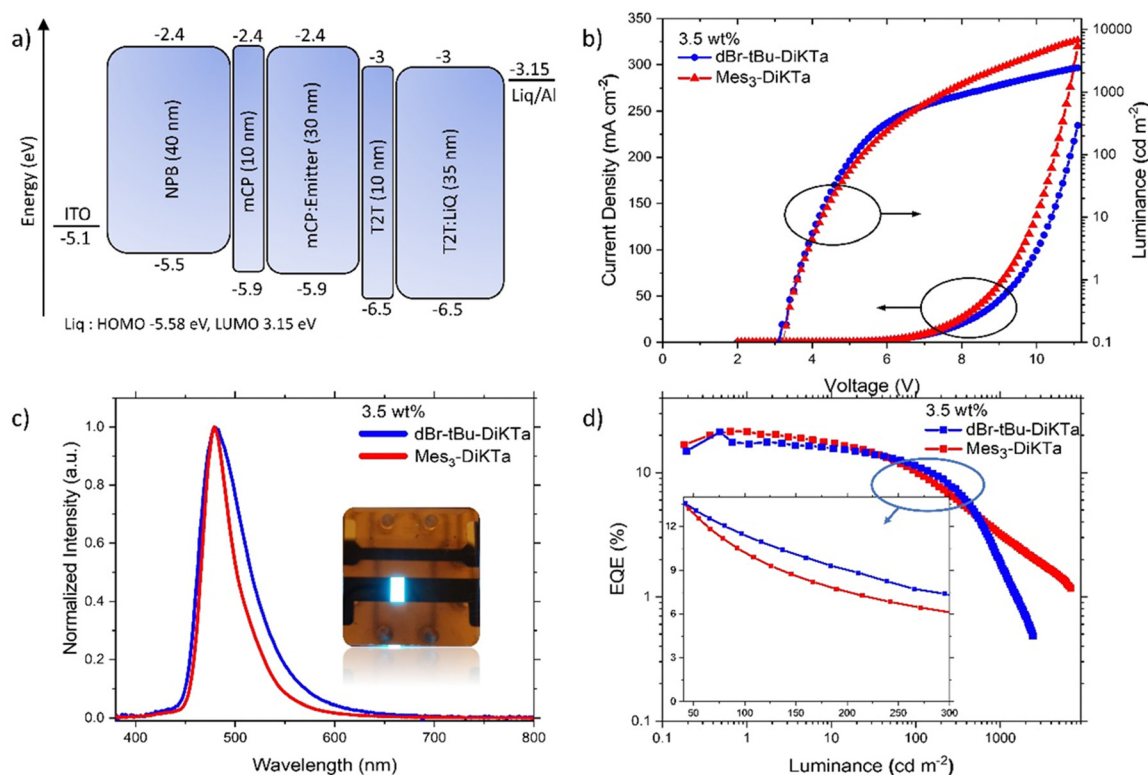
This journal is © The Royal Society of Chemistry 2024

J. Mater. Chem. C, 2024, **12**, 1996–2006 | **2003**

Fig. 7 OLEDs JVL results. (a) Device architecture, (b) JVL curves, (c) EL spectra and (d) EQE *vs.* luminance of **dBr-*t*Bu-DiKTa** (blue) and **Mes₃-DiKTa** (red). Inset in figure (d): linear EQE *vs.* luminance to highlight the roll-off difference in the noted region.

Φ_{PL}, we assign the high EQE value and broader EL spectrum to its exciplex contribution with the mCP host. The **dBr-*t*Bu-DiKTa** OLEDs show higher luminance up to a specific voltage (7 V), which correlates with improved EQE roll-off behaviour up to this specific region. This improved performance is attributed to the HAE that enhances SOC and thus k_{RISC}, enabling more efficient triplet harvesting. Any additional triplet harvesting channels from the exciplex species, that could also improve the device roll-off but were not clearly visible in the photophysical measurements (because monomer, aggregate and exciplex species emission complicate the results), must be acknowledged. At a luminance of 500 cd m⁻² (current density of 4 mA cm⁻²) there is a critical point at which the efficiency roll-off of the OLED with **dBr-*t*Bu-DiKTa** becomes much worse than the device with **Mes₃-DiKTa** (EQE_{500} = 6% in both cases, at the crossover point). This effect is possibly a combination of detrimental effects such as weaker C–Br bonds leading to degradation, or increased activity of the aggregate species that sterically shielded **Mes₃-DiKTa** which is more resistant towards forming.

To explore the effect of emitter aggregation on the device efficiency roll-off, additional devices with **dBr-*t*Bu-DiKTa** at 1 wt% loading were fabricated, and the results are shown in Fig. S28 (ESI†). There is a minor hypsochromic shift of the EL spectrum, accompanied by a narrower FWHM indicating that the intermolecular species EL contribution is reduced. However, intermolecular interactions remain as evidenced by

comparison of the EL spectrum to the 0.1 wt% zeonex film PL spectra (Fig. 3(b), and Fig. S28a, ESI†). The electrical response of the device is worse at lower concentrations (Fig. S28b, ESI†), resulting in a decreased EQE_{max} of 17.9% and increased efficiency roll-off up to 4 mA cm⁻². Comparing the two **dBr-*t*Bu-DiKTa** devices above 4 mA cm⁻² (Fig. S28e, ESI†), the efficiency roll-off appears stronger in the 3.5 wt% device while the efficiency roll-off profile of the 1 wt% resembles more closely that of the **Mes₃DiKTa** OLED. The latter observation indicates that among other detrimental factors, guest–guest aggregation quenching plays an important role at higher current densities.

Conclusions

From these results it is possible to understand the competing effects imparted by peripheral bromine substitution on the emission energy and decay lifetimes of the **DiKTa** derivatives (Table 1 and Fig. 4). **Mes₃-DiKTa** has the slowest PF and DF emission in both investigated hosts. The kinetics of both PF and DF emission are significantly enhanced by SOC associated with the increasing bromine content in **dBr-*t*Bu-DiKTa** and **tBr-DiKTa**. The peripheral mesityl decoration in **Mes₃-DiKTa**, however, suppresses intermolecular interactions that are prevalent in the bromine-substituted emitters, resulting in significant aggregate emission in the latter and likely lowering the Φ_{PL} values in the zeonex host. The complexity of the intermolecular

2004 | *J. Mater. Chem. C*, 2024, **12**, 1996–2006

This journal is © The Royal Society of Chemistry 2024

interactions and the resulting photophysics is further increased in the mCP host, where an extra exciplex species appears to enhance the Φ_{PL} compared to the inert zeonex host.

The low Φ_{PL}, along with the strong intermolecular interactions, even at 0.1 wt% loading, are prohibitive factors for the use of **tBr-DiKTa** in OLEDs. Comparing the devices with **dBr-tBu-DiKTa** and **Mes₃-DiKTa** reveals the impact of bromine substitution on the improved k_{RISC} and the lower efficiency roll-off. Despite some indications of EL from aggregates, the device EQEs are nearly identical at low current densities, and the EQE roll-off (up to 4 mA cm^{-2}) was reduced in the OLED with **dBr-tBu-DiKTa**, indicating improved triplet harvesting up to this critical current density, being in good agreement with the estimated k_{RISC} calculation. Beyond that critical current density, we suggest that SOC-assisted ISC for **dBr-tBu-DiKTa** leads to a build-up of the triplet exciton population in the EML, resulting in more severe roll-off compared to the device with **Mes₃-DiKTa**. A comparison of 1 and 3.5 wt% **dBr-tBu-DiKTa** devices shows that the impact of aggregation is mitigated to some extent, although other detrimental parameters contribute to the overall efficiency roll-off in these devices (Table S1, ESI†) when the emitter loading is too low. It appears, therefore, that the effect of peripheral heavy halogen atoms on the performance of MR-TADF OLEDs – both directly in terms of affecting k_{RISC} by enhancing SOC through the HAE, and indirectly through intermolecular interactions – can be both positive or negative depending on the exciton density.

Conflicts of interest

There are no conflicts to declare.

Acknowledgements

References

1 F. B. Dias, K. N. Bourdakos, V. Jankus, K. C. Moss, K. T. Kamtekar, V. Bhalla, J. Santos, M. R. Bryce and A. P. Monkman, *Adv. Mater.*, 2013, **25**, 3707–3714.

2 S. Y. Lee, T. Yasuda, Y. S. Yang, Q. Zhang and C. Adachi, *Angew. Chem., Int. Ed.*, 2014, **53**, 6402–6406.

3 G. Hong, X. Gan, C. Leonhardt, Z. Zhang, J. Seibert, J. M. Busch and S. Brase, *Adv. Mater.*, 2021, **33**, 2005630.

4 M. A. Baldo, D. F. O'Brien, Y. You, A. Shoustikov, S. Sibley, M. E. Thompson and S. R. Forrest, *Nature*, 1998, **395**, 151–154.

5 X. Xu, X. Yang, J. Zhao, G. Zhou and W. Y. Wong, *Asian J. Org. Chem.*, 2015, **4**, 394–429.

6 F. B. Dias, T. J. Penfold and A. P. Monkman, *Methods Appl. Fluoresc.*, 2017, **5**, 012001.

7 J. Gibson, A. P. Monkman and T. J. Penfold, *ChemPhysChem*, 2016, **17**, 2956–2961.

8 P. K. Samanta, D. Kim, V. Coropceanu and J.-L. Brédas, *J. Am. Chem. Soc.*, 2017, **139**, 4042–4051.

9 K. R. Naveen, P. Palanisamy, M. Y. Chae and J. H. Kwon, *Chem. Commun.*, 2023, **59**, 3685–3702.

10 Y. Kondo, K. Yoshiura, S. Kitera, H. Nishi, S. Oda, H. Gotoh, Y. Sasada, M. Yanai and T. Hatakeyama, *Nat. Photonics*, 2019, **13**, 678–682.

11 S. Oda, B. Kawakami, Y. Yamasaki, R. Matsumoto, M. Yoshioka, D. Fukushima, S. Nakatsuka and T. Hatakeyama, *J. Am. Chem. Soc.*, 2022, **144**, 106–112.

12 X. Lv, J. Miao, M. Liu, Q. Peng, C. Zhong, Y. Hu, X. Cao, H. Wu, Y. Yang, C. Zhou, J. Ma, Y. Zou and C. Yang, *Angew. Chem., Int. Ed.*, 2022, **61**, e202201588.

13 X. Song, S. Shen, S. Zou, F. Guo, Y. Wang, S. Gao and Y. Zhang, *Chem. Eng. J.*, 2023, **467**, 143557.

14 Y. Qi, W. Ning, Y. Zou, X. Cao, S. Gong and C. Yang, *Adv. Funct. Mater.*, 2021, **31**, 2102017.

15 Y. Xu, C. Li, Z. Li, Q. Wang, X. Cai, J. Wei and Y. Wang, *Angew. Chem., Int. Ed.*, 2020, **59**, 17442–17446.

16 M. Yang, I. S. Park and T. Yasuda, *J. Am. Chem. Soc.*, 2020, **142**, 19468–19472.

17 M. A. Baldo, S. Lamansky, P. E. Burrows, M. E. Thompson and S. R. Forrest, *Appl. Phys. Lett.*, 1999, **75**, 4–6.

18 A. Kretzschmar, C. Patze, S. T. Schwaebel and U. H. F. Bunz, *J. Org. Chem.*, 2015, **80**, 9126–9131.

19 H. S. Kim, J. Y. Lee, S. Shin, W. Jeong, S. H. Lee, S. Kim, J. Lee, M. C. Suh and S. Yoo, *Adv. Funct. Mater.*, 2021, **31**, 2104646.

20 L. G. Franca, Y. Long, C. Li, A. Danos and A. Monkman, *J. Phys. Chem. Lett.*, 2021, **12**, 1490–1500.

21 J. Xu, X. Zhu, J. Guo, J. Fan, J. Zeng, S. Chen, Z. Zhao and B. Z. Tang, *ACS Mater. Lett.*, 2019, **1**, 613–619.

22 Y. Liu, L. Hua, Z. Zhao, S. Ying, Z. Ren and S. Yan, *Adv. Sci.*, 2021, **8**, 2101326.

23 D. de Sa Pereira, D. R. Lee, N. A. Kukhta, K. H. Lee, C. L. Kim, A. S. Batsanov, J. Y. Lee and A. P. Monkman, *J. Mater. Chem. C*, 2019, **7**, 10481–10490.

24 S. Schott, E. R. McNellis, C. B. Nielsen, H.-Y. Chen, S. Watanabe, H. Tanaka, I. McCulloch, K. Takimiya, J. Sinova and H. Sirringhaus, *Nat. Commun.*, 2017, **8**, 15200.

25 B. H. Drummond, G. C. Hoover, A. J. Gillett, N. Aizawa, W. K. Myers, B. T. McAllister, S. T. E. Jones, Y.-J. Pu, D. Credgington and D. S. Seferos, *J. Phys. Chem. C*, 2020, **124**, 6364–6370.

26 X. Han, X. Wang, Y. Wu, J. Zhao, Y. Liu, H. Shu, X. Wu, H. Tong and L. Wang, *J. Mater. Chem. C*, 2022, **10**, 7437–7442.

27 Y. Ren, Y. Wada, K. Suzuki, Y. Kusakabe, J. Geldsetzer and H. Kaji, *Appl. Phys. Express*, 2021, **14**, 071003.

28 N. Kanno, Y. Ren, Y. Kusakabe, K. Suzuki, K. Shizu, H. Tanaka, Y. Wada, H. Nakagawa, J. Geldsetzer and H. Kaji, *Appl. Phys. Express*, 2023, **16**, 011006.

29 K. Shizu, Y. Ren and H. Kaji, *J. Phys. Chem. A*, 2023, **127**, 439–449.

This journal is © The Royal Society of Chemistry 2024

J. Mater. Chem. C, 2024, **12**, 1996–2006 | **2005**

30 D. Zhang, C. Jiang, Z. Wen, X. Feng and K. Li, *Chem. – Eur. J.*, 2022, **28**, e202202305.

31 Y. Wang, W. Ning, W. Yang, L. Li, N. Li, T. Liu, S. Gong, X. Gao and C. Yang, *Dyes Pigm.*, 2023, **214**, 111225.

32 S. Madayanad Suresh, D. Hall, D. Beljonne, Y. Olivier and E. Zysman-Colman, *Adv. Funct. Mater.*, 2020, **30**, 1908677.

33 M. K. Etherington, J. Gibson, H. F. Higginbotham, T. J. Penfold and A. P. Monkman, *Nat. Commun.*, 2016, **7**, 13680.

34 K. Stavrou, A. Danos, T. Hama, T. Hatakeyama and A. Monkman, *ACS Appl. Mater. Interfaces*, 2021, **13**, 8643–8655.

35 F. Chen, L. Zhao, X. Wang, Q. Yang, W. Li, H. Tian, S. Shao, L. Wang, X. Jing and F. Wang, *Sci. China: Chem.*, 2021, **64**, 547–551.

36 I. S. Park, H. Min and T. Yasuda, *Angew. Chem., Int. Ed.*, 2022, **61**, e202205684.

37 Q. Li, Y. Wu, Q. Yang, S. Wang, S. Shao and L. Wang, *ACS Appl. Mater. Interfaces*, 2022, **14**, 49995–50003.

38 L. Yang, P. Wang, K. Zhang, S. Wang, S. Shao and L. Wang, *Dyes Pigm.*, 2023, **216**, 111371.

39 X. Cao, K. Pan, J. Miao, X. Lv, Z. Huang, F. Ni, X. Yin, Y. Wei and C. Yang, *J. Am. Chem. Soc.*, 2022, **144**, 22976–22984.

40 D. Li, M. Li, D. Liu, J. Yang, W. Li, Z. Yang, H. Yuan, S. Jiang, X. Peng and G. X. Yang, *Adv. Opt. Mater.*, 2023, 2301084.

41 T. Hua, L. Zhan, N. Li, Z. Huang, X. Cao, Z. Xiao, S. Gong, C. Zhou, C. Zhong and C. Yang, *Chem. Eng. J.*, 2021, **426**, 131169.

42 Y. X. Hu, J. Miao, T. Hua, Z. Huang, Y. Qi, Y. Zou, Y. Qiu, H. Xia, H. Liu, X. Cao and C. Yang, *Nat. Photonics*, 2022, **16**, 803–810.

43 S. M. Pratik, V. Coropceanu and J.-L. Brédas, *ACS Mater. Lett.*, 2022, **4**, 440–447.

44 S. M. Pratik, V. Coropceanu and J.-L. Brédas, *Chem. Mater.*, 2022, **34**, 8022–8030.

45 Y. Li, W. Li, J. Hu, X. Yao, L. Hua, W. Cai, S. Shi, C. Zhang, Z. Liu and S. Li, *Adv. Opt. Mater*, 2023, **11**, 2300298.

46 F. Huang, Y.-C. Cheng, H. Wu, X. Xiong, J. Yu, X.-C. Fan, K. Wang and X.-H. Zhang, *Chem. Eng. J.*, 2023, **465**, 142900.

47 Y. Hu, J. Miao, C. Zhong, Y. Zeng, S. Gong, X. Cao, X. Zhou, Y. Gu and C. Yang, *Angew. Chem., Int. Ed.*, 2023, **62**, e202302478.

48 D. Hall, S. M. Suresh, P. L. dos Santos, E. Duda, S. Bagnich, A. Pershin, P. Rajamalli, D. B. Cordes, A. M. Z. Slawin, D. Beljonne, A. Köhler, I. D. W. Samuel, Y. Olivier and E. Zysman-Colman, *Adv. Opt. Mater.*, 2020, **8**, 1901627.

49 C. Adamo and V. Barone, *J. Chem. Phys.*, 1999, **110**, 6158–6170.

50 T. H. Dunning, Jr., *J. Chem. Phys.*, 1989, **90**, 1007–1023.

51 I. Kim, K. H. Cho, S. O. Jeon, W. J. Son, D. Kim, Y. M. Rhee, I. Jang, H. Choi and D. S. Kim, *JACS Au*, 2021, **1**, 987–997.

52 J. M. Kaminski, A. Rodriguez-Serrano, F. Dinkelbach, H. Miranda-Salinas, A. P. Monkman and C. M. Marian, *Chem. Sci.*, 2022, **13**, 7057–7066.

53 A. Pershin, D. Hall, V. Lemaur, J. C. Sancho-Garcia, L. Muccioli, E. Zysman-Colman, D. Beljonne and Y. Olivier, *Nat. Commun.*, 2019, **10**, 597.

54 D. Hall, J. C. Sancho-García, A. Pershin, G. Ricci, D. Beljonne, E. Zysman-Colman and Y. Olivier, *J. Chem. Theory Comput.*, 2022, **18**, 4903–4918.

55 S. Wu, W. Li, K. Yoshida, D. Hall, S. Madayanad Suresh, T. Sayner, J. Gong, D. Beljonne, Y. Olivier, I. D. W. Samuel and E. Zysman-Colman, *ACS Appl. Mater. Interfaces*, 2022, **14**, 22341–22352.

56 D. Sun, S. M. Suresh, D. Hall, M. Zhang, C. Si, D. B. Cordes, A. M. Z. Slawin, Y. Olivier, X. Zhang and E. Zysman-Colman, *Mater. Chem. Front.*, 2020, **4**, 2018–2022.

57 Y. Zhang, D. Zhang, J. Wei, X. Hong, Y. Lu, D. Hu, G. Li, Z. Liu, Y. Chen and L. Duan, *Angew. Chem., Int. Ed.*, 2020, **59**, 17499–17503.

58 Y. Tsuchiya, S. Diesing, F. Bencheikh, Y. Wada, P. L. Dos Santos, H. Kaji, E. Zysman-Colman, I. D. W. Samuel and C. Adachi, *J. Phys. Chem. A*, 2021, **125**, 8074–8089.

59 K. Stavrou, L. G. Franca and A. P. Monkman, *ACS Appl. Electron. Mater.*, 2020, **2**, 2868–2881.

60 D. K. A. Phan Huu, S. Saseendran, R. Dhali, L. G. Franca, K. Stavrou, A. Monkman and A. Painelli, *J. Am. Chem. Soc.*, 2022, **144**, 15211–15222.

61 H. Miranda-Salinas, Y.-T. Hung, Y.-S. Chen, D. Luo, H.-C. Kao, C.-H. Chang, K.-T. Wong and A. Monkman, *J. Mater. Chem. C*, 2021, **9**, 8819–8833.

62 P. L. dos Santos, J. S. Ward, M. R. Bryce and A. P. Monkman, *J. Phys. Chem. Lett.*, 2016, **7**, 3341–3346.

63 G. Méhes, K. Goushi, W. J. Potscavage Jr. and C. Adachi, *Org. Electron.*, 2014, **15**, 2027–2037.

64 K. Stavrou, S. Madayanad Suresh, D. Hall, A. Danos, N. A. Kukhta, A. M. Z. Slawin, S. Warriner, D. Beljonne, Y. Olivier, A. Monkman and E. Zysman-Colman, *Adv. Opt. Mater.*, 2022, **10**, 2200688.

65 M. K. Etherington, N. A. Kukhta, H. F. Higginbotham, A. Danos, A. N. Bismillah, D. R. Graves, P. R. McGonigal, N. Haase, A. Morherr, A. S. Batsanov, C. Pflumm, V. Bhalla, M. R. Bryce and A. P. Monkman, *J. Phys. Chem. C*, 2019, **123**, 11109–11117.

66 X. Wu, B.-K. Su, D.-G. Chen, D. Liu, C.-C. Wu, Z.-X. Huang, T.-C. Lin, C.-H. Wu, M. Zhu, E. Y. Li, W.-Y. Hung, W. Zhu and P.-T. Chou, *Nat. Photonics*, 2021, **15**, 780–786.

67 L. Zhang, Y.-X. Zhang, Y. Hu, X.-B. Shi, Z.-Q. Jiang, Z.-K. Wang and L.-S. Liao, *ACS Appl. Mater. Interfaces*, 2016, **8**, 16186–16191.

2006 | *J. Mater. Chem. C*, 2024, **12**, 1996–2006

This journal is © The Royal Society of Chemistry 2024